A Thesis Submitted to the Sylhet Engineering College for the Degree of
Bachelor of Science in Electrical and Electronic Engineering

Design and Analysis of Optical Tractor Beam for Rayleigh Particles Using an Anisotropic Metasurface

By
Fahim Shahriar Chowdhury
Iftekhar Hossain
&
Amio Chakraborty

Supervised by
Md. Janibul Alam Soeb
Assistant Professor

Department of Farm Power and Machinery

Faculty of Agricultural Engineering and Technology
Sylhet Agricultural University, Sylhet

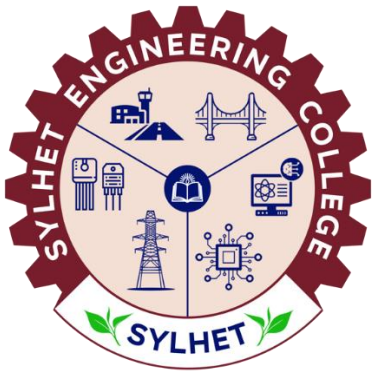

June, 2025
Sylhet Engineering College, Sylhet
Affiliated with
Shahjalal University of Science & Technology (SUST)

CERTIFICATION

The thesis titled **"Optical Tractor Beam using Anisotropic Metasurface for Rayleigh particles"** submitted by **Fahim Shahriar Chowdhury**, **Iftekhar Hossain** and **Amio Chakraborty**; Student ID: **2019338541**, **2019338555 and 2019338560** ; Session **2019-2020**, to the Department of Electrical and Electronic Engineering, Sylhet Engineering College, has been accepted as satisfactory in partial fulfillment of the requirement for the Degree of Bachelor of Science in Electrical and Electronic Engineering and approved as to its style and contents.

BOARD OF EXAMINERS

_____

Md. Shahid Iqbal — Chairman
Assistant Professor and Head
Department of Electrical and Electronic Engineering
Sylhet Engineering College, Sylhet.

_____

MD. Janibul Alam Soeb — Supervisor
Assistant Professor
Department of Farm Power and Machinery
Shahjalal University of Science & Technology, Sylhet

_____

Salman Fazle Rabby — Member
Lecturer
Department of Electrical and Electronic Engineering
Sylhet Engineering College, Sylhet.

_____

Apurba Biswas — Member
Assistant Professor
Department of Electrical and Electronic Engineering
Sylhet Engineering College, Sylhet.

_____

Md. Ashraful Alam — Member
Lecturer
Department of Electrical and Electronic Engineering
Sylhet Engineering College, Sylhet.

Mahedi Kamal Ahmed
Lecturer — Member
Department of Electrical and Electronic Engineering
Sylhet Engineering College, Sylhet.

Arif Ahammad — Member (External)
Assistant Professor
Department of Electrical and Electronic Engineering
Shahjalal University of Science & Technology, Sylhet.

Acknowledgement

We begin by extending our gratitude to the Almighty, whose guidance and sustenance have enabled us to embark on this journey and complete the requirements for the Bachelor of Science in Electrical and Electronics Engineering (EEE), including our thesis work. It is through His grace that we have attained the strength and determination to achieve this milestone.

We would like to express our sincere appreciation to our esteemed supervisor, **Md. Janibul Alam Soeb,** Assistant Professor, Department of FPM (Farm Power and Machinery), Faculty of Agricultural Engineering and Technology, Sylhet Agricultural University. His invaluable academic mentorship, exemplary leadership, positive encouragement, insightful advice, and unwavering support have been instrumental throughout our academic pursuit. We are truly grateful for his guidance. Furthermore, it is an honor to express our gratitude to our head of dept. **Md. Shahid Iqbal** and other faculty members, **Salman Fazle Rabby, Md. Ashraful Alam**, **Apurba Biswas And Mahedi Kamal Ahmed** for their kindness, support, and cooperation during our academic journey. Their assistance has been greatly appreciated. Our heartfelt gratitude also goes to our parents, siblings, classmates, and friends in the EEE department at SEC. We acknowledge the sacrifices, prayers, encouragement, and unwavering support they have provided, which have contributed significantly to our success. We are indebted to them for their role in shaping our academic and personal development.

Abstract

This thesis presents a comprehensive study on the design and implementation of optical tractor beams utilizing anisotropic metasurfaces to manipulate Rayleigh particles. By exploiting the direction-dependent electromagnetic properties of metasurfaces, composed of alternating plasmonic and dielectric layers, the study achieves precise control over light fields to generate negative radiation forces, enabling the pulling of subwavelength particles toward the light source. A robust theoretical framework models the interaction between structured light fields and Rayleigh particles, focusing on gradient and scattering forces. Numerical simulations, conducted using COMSOL Multiphysics, validate the metasurface designs, demonstrating stable optical pulling forces across a frequency range of 500–1500 THz for dielectric, plasmonic, and chiral particles. Experimental feasibility is assessed through proposed setups, emphasizing practical fabrication and characterization methods. The results reveal frequency-dependent force profiles, with significant pulling forces attributed to multipole interference, particularly electric and magnetic dipole interactions. This work advances optical manipulation techniques, offering transformative potential for nanotechnology, biophysics, and optical sorting applications through compact, scalable metasurface-based systems.

Keywords: Optical tractor beam, Anisotropic metasurface, Rayleigh particles, Optical forces, Electromagnetic field manipulation, Numerical simulations, Nanotechnology, Optical sorting.

Table of Contents

List of Figures

List of Tables

Chapter 1: Introduction

1.1 Overview

Optical tractor beams are innovative light-based systems that defy conventional optics by pulling particles toward the light source, rather than pushing them away via radiation pressure. This capability stems from carefully engineered electromagnetic fields that create negative radiation forces. Anisotropic metasurfaces two-dimensional arrays of subwavelength structures with direction-dependent optical properties-offer a powerful platform for designing such beams. These metasurfaces enable precise control over light's wavefront, polarization, and intensity, making them ideal for manipulating Rayleigh particles (particles much smaller than the light's wavelength) through tailored optical forces. Rayleigh particles, due to their small size, interact with light primarily through scattering and absorption, influenced by their polarizability. Optical tractor beams using anisotropic metasurfaces can generate gradient and non-gradient forces to attract and trap these particles, offering applications in fields like targeted single-molecule studies, and nanoscale assembly. Unlike traditional tractor beam setups, which often require complex optical systems like Bessel beams or holography, metasurfaces provide a compact, tunable, and efficient alternative.

This thesis investigates the design and implementation of metasurface-based tractor beams, focusing on theoretical modeling, numerical simulations, and experimental validation to achieve stable, long-range manipulation of Rayleigh particles, advancing the frontier of optical control in nanotechnology.

1.2 Anisotropic Metasurfaces

Metasurfaces are two-dimensional arrays of subwavelength nanostructures designed to manipulate electromagnetic waves with unprecedented control. Unlike bulk optical components, metasurfaces offer a compact, planar platform for tailoring light's properties, including phase, amplitude, and polarization. Anisotropic metasurfaces, in particular, exhibit direction-dependent electromagnetic responses, enabling the creation of complex wavefronts and force fields. By carefully designing the geometry and material properties of metasurface elements, researchers can engineer light fields with specific characteristics, such as non-diffracting beams or asymmetric force profiles, which are critical for tractor beam functionality.

In the context of optical tractor beams, anisotropic metasurfaces serve as a transformative tool. They allow for the generation of structured light fields that can induce pulling forces on particles by manipulating the local electromagnetic field. For example, a metasurface can be designed to convert an incident plane wave into a Bessel-like beam with a tailored phase gradient, enabling the creation of a tractor beam with enhanced stability and range.

1.3 Rayleigh Particles

Rayleigh particles are objects with dimensions much smaller than the wavelength of the incident light, typically on the order of tens of nanometers. In this regime, the particle's interaction with light is dominated by electric dipole scattering, described by the Rayleigh scattering theory. The optical forces acting on Rayleigh particles are generally weak due to their small polarizability, posing significant challenges for manipulation. However, these particles are of great interest in nanotechnology and biophysics, as they include entities like nanoparticles, biomolecules, and quantum dots. The manipulation of Rayleigh particles using optical tractor beams requires precise control over the light field to overcome the weak scattering forces. Anisotropic metasurfaces offer a solution by enabling the creation of highly localized and intense field gradients, which can enhance the optical forces acting on these particles.

1.4 Objectives

The primary objectives are to design, analyze, and optimize optical tractor beams using anisotropic metasurfaces for the manipulation of Rayleigh particles. The specific goals are as follows:

1. To design a multilayer non-planar anisotropic metasurface capable of generating structured optical fields that can exert pulling forces on Rayleigh particles.
2. To simulate and evaluate the behavior of optical pulling forces acting on different nanoparticle types across 500–1500 THz using COMSOL Multiphysics.
3. To validate the metasurface's ability to produce stable, direction-specific optical pulling forces through multipole interference and surface current analysis.

1.5 Significance

The significance of this field of optical manipulation by introducing a novel approach to optical tractor beams using anisotropic metasurfaces. The ability to control Rayleigh particles with precision has far-reaching implications across multiple disciplines:

1. **Nanotechnology**: Metasurface-based tractor beams could enable precise assembly and positioning of nanoparticles for the fabrication of advanced materials, such as photonic crystals or plasmonic devices. This could lead to breakthroughs in nanoscale manufacturing and device integration.
2. **Biophysics and Biomedicine:** The non-contact manipulation of biomolecules, such as proteins or DNA, in the Rayleigh regime could revolutionize targeted drug delivery and single-molecule studies. Tractor beams offer a gentle, non-invasive method for transporting delicate biological entities without physical contact.
3. **Optical Sorting and Sensing**: The ability to selectively manipulate Rayleigh particles based on their optical properties could enhance optical sorting techniques, which are critical for applications in diagnostics and environmental monitoring. Metasurfaces could enable high-throughput, label-free sorting of nanoparticles.
4. **Fundamental Science**: This research contributes to the fundamental understanding of light-matter interactions in the Rayleigh regime, particularly the role of non-conservative forces in optical manipulation. By leveraging metasurfaces, the study explores new regimes of optical force dynamics, potentially uncovering novel physical phenomena.
5. **Technological Innovation**: The development of compact, planar metasurface-based tractor beams could lead to scalable and cost-effective optical manipulation systems. Unlike traditional bulky optics, metasurfaces offer a lightweight, integrable platform that could be incorporated into lab-on-chip devices or portable diagnostic tools.

1.6 Thesis Structure

This thesis is organized into six chapters to systematically explore the design, simulation, and implications of optical tractor beams using anisotropic metasurfaces for manipulating Rayleigh particles. The structure is as follows:

Chapter 1: Covers optical tractor beams, anisotropic metasurfaces, Rayleigh particles, objectives, and significance in nanotechnology and biophysics.

Chapter 2: Literature Review Summarizes prior work on optical pulling, tweezers, chirality, and beam-based manipulation, with references.

Chapter 3: Describes COMSOL simulations, anisotropic metasurface design, nanoparticle setup, laser parameters, and force calculations.

Chapter 4: Analyzes frequency-dependent forces, mechanisms, and applications, comparing with isotropic designs.

Chapter 5: Recaps contributions and suggests future research in broadband, tunable, and application-specific tractor beams.

1.7. Summary

This chapter provides an overview of optical tractor beams, which use engineered light fields to pull particles toward the source, contrasting with traditional radiation pressure that pushes them away. It introduces anisotropic metasurfaces as a compact platform for manipulating Rayleigh particles (subwavelength objects like nanoparticles) through tailored electromagnetic properties. Key sections discuss metasurface design for wavefront control, Rayleigh particle interactions via scattering, and the thesis objectives: designing metasurfaces for pulling forces, simulating forces on various nanoparticles across 500–1500 THz using COMSOL, and validating stability via multipole interference. The significance is highlighted in applications like nanotechnology, biophysics, optical sorting, and fundamental light-matter studies, emphasizing metasurfaces' advantages over bulky optics.

Chapter 2: Literature Review

Over the last few decades, many researchers have made great contributions into the understanding of optical pulling force and tractor beams. In this section, some of these experiments and models are summarized. The summaries represent the methods and the significances of those experiments. For a detailed understanding of the experiments, the reader is referred to the cited references.

Arthur Ashkin et al. [1] introduced the concept of optical tweezers, a technique using laser radiation pressure to trap and manipulate microscopic objects, including atoms, molecules and biological cells. This technology which he pioneered in the late 1960s, revolutionized various fields, especially biology and physics. This work led to the development of optical trapping, a cornerstone of modern optical manipulation techniques. **Chen** et al. [2] pioneered gradient-less optical pulling forces, enabling the manipulation of particles in the negative force regime. This research explores how resonance effects in optical manipulation can be used to create structural order and achieve selective manipulation of nanoscale materials, including sorting and isolating targets under different quantum resonance conditions. This work focuses on manipulating matter using heat-mediated optical forces, allowing for more versatile control of various compositions, shapes and sizes of materials.

Sergey Sukhov & Aristide Dogariu et al. [3] conducted a comparative analysis of the role of chirality in optical forces, particularly when interacting with circularly polarized or vortex beams. This work opened new avenues for the manipulation of chiral particles. Their research evaluates that the generation of non-conservative optical forces that act in a direction opposite to the propagation of the incident beam. The concept can be applied to tailor the force fields produced on non-absorbing bodies regardless of their sizes and shapes. **Andrey V. Novitsky & Denis V. Novitsky** et al. [4] theoretically demonstrated the negative components of energy flux of vector bessel beams that predicts the optical pulling of a particle. They referred the vector bessel beams as the superposition of TE and TM-polarized electromagnetic bessel beams. The interference produces a complex energy flux. The analytical calculation unveils that the resultant poynting power has only the longitudinal (i.e. S_z) and azimuthal components (i.e. $S_ø$) which results in a vanishing optical force in the radial direction.

Lee, Roicman and Grier et al. [5] predicted optical solenoidal beams those have an interesting feature of pulling a particle in the direction opposite to the energy propagation direction. An infinite line of light wave propagating in the optical axis was considered to design the solenoid

beam. The derivation reveals the formation of the solenoid beams due to the superposition of the m-th order bessel beams. Helical pitch and spiral pitch are two of the most important features of a solenoid beam. The experimental observation of the radiation pressure on silica spheres dispersed in water exibits the direct dependence of the force direction on the helical and spiral pitch of the solenoid beam. The experimental observation of the radiation pressure on silica spheres dispersed in water exibits the direct dependence of the force direction on the helical and spiral pitch of the solenoid beam. **Ruffner and Grier** et al. [6] experimentally illustrated an active tractor beam formed due to the superposition of two coaxial bessel beams. The two beams differ in their longitudinal wave numbers and relative phase. For the demonstration, a sample of silica particle was used to observe the forces on it. Silica particles were trapped in the beam axis. The particles can be pulled or pushed along the beam axis by varying the relative phase between the two beams. This tractor beam outperforms optical tweezers in terms of stable axial trapping.

Kajorndejnukul et al. [7] experimentally demonstrated the optical pulling of any arbitrary shaped objects in a dielectric fluid is possible using paraxial beams. Optical force on small drops of donecane particles, illuminated by paraxial beams, placed at the interface between air and water was determined. The theory reveals the direct dependence of optical forces on the shape and optical properties of the particles. Increase in the forward momentum results in optical pulling of the particle. **M.Mansuripur** et al. [8] revealed optical pulling of particles by the magnification of photon linear momentum. The magnitude of linear momentum is directly proportional to the energy and inversely proportional to the speed of light wave. The force on a prism in free space can be predicted. Calculation of force by the change of momentum method is very much complicated when the prism is immersed in a fluid. The calculation of force acting on a particle, immersed in a fluid, using the momentum exchange effect gives rise to the Abraham-Minkowski debate. The most reliable method is to use the Lorentz force theorem for the calculation of total force.

2.1 Summary

This chapter reviews key contributions to optical pulling forces and tractor beams. It covers foundational work like Arthur Ashkin's optical tweezers for trapping microscopic objects, Chen et al.'s gradient-less pulling via resonance for nanoscale manipulation, and Sukhov & Dogariu's analysis of chirality in forces with circularly polarized beams. Other studies include Novitsky et al.'s vector Bessel beams for negative energy flux, Lee et al.'s solenoidal beams with helical pitch-dependent pulling, Ruffner & Grier's coaxial Bessel beam superposition for active tractor

beams, Kajorndejnukul et al.'s pulling of arbitrary shapes in fluids, and Mansuripur et al.'s momentum magnification in prisms. The summaries emphasize methods, significance, and references for deeper reading.

Chapter 3: Methodology

3.1 Overview

This chapter outlines the comprehensive methodology adopted to investigate the generation of optical pulling forces on Rayleigh particles positioned over an anisotropic metasurface substrate. The study employs full-wave numerical simulations to evaluate the behavior of nanoparticles under the influence of a time-harmonic plane-polarized laser beam. The methodology is structured around the design of the anisotropic substrate, positioning of the nano particle, simulation tools, environmental conditions, and the mathematical computation of optical force using Maxwell's stress tensor.

3.2 Simulation Environment and tools

All simulations in this study are conducted using COMSOL Multiphysics 6.2, a finite element-based Multiphysics simulation software. The Radio Frequency (RF) Module is used for solving the full-wave frequency -domain Maxwell's equations. This environment enables detailed modeling of complex material structures such as multilayer Hyperbolic Metamaterials and anisotropic nanostructures with nanometer-scale resolution.

COMSOL's essential modules utilized in this study include

1. 3D electromagnetic wave simulation,
2. Accurate meshing in high index contrast regions,
3. Custom material definition,
4. Boundary conditions to mimic open-space environments using Perfectly Matched Layers (PMLs).

3.3 Substrate Design and Material Selection

In this study, the substrate plays a critical role in mediating light-matter interactions and enhancing optical pulling force. The chosen substrate is a non-planar multilayered anisotropic metasurface constructed from alternating plasmonic and dielectric layers. This non-planer multilayered structure modifies field distributions directionally, resulting in polarization gradients, asymmetric scattering, tailored reflection/transmission.

Material Selection

1. **Plasmonic Material (P):**

Material: Silver (Ag), Aluminum (Al)

Properties: Strong negative real permittivity in the visible and near-infrared range, suitable for supporting surface plasmon polaritons (SPPs)

Optical Constants: Taken from experimental data by Johnson and Christy.

2. **Dielectric Material (D):**

Material: Silicon Dioxide (SiO_2)

Properties: Low-loss transparent dielectric with a relatively constant refractive index n=1.45 in the optical regime.

Function: Provides contrast in permittivity and enables anisotropy when alternated with Silver.

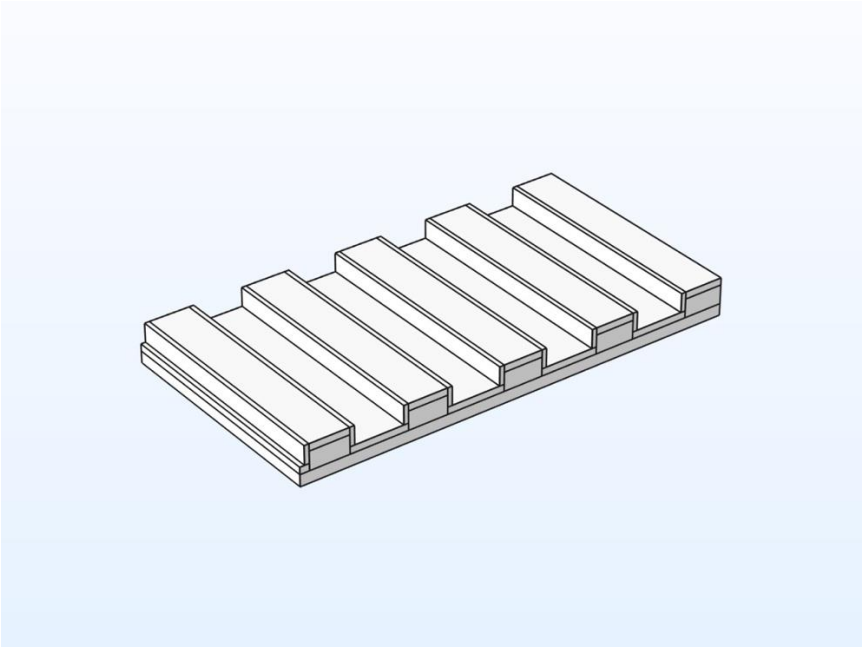

Figure 3.1. Anisotropic Substrate Geometry Used in COMSOL Simulation.

The above figure illustrates the 3D geometry of the anisotropic substrate designed for the COMSOL Multiphysics simulation. The structure consists of periodic ridges aligned along a single axis, forming a grating-like pattern on a dielectric base. This engineered anisotropy introduces direction-dependent optical responses, which are critical for manipulating light–matter interactions at the nanoscale. In the context of this study, the anisotropic substrate is employed to generate optical pulling forces (tractor beam effects) on subwavelength particles placed near the surface. The periodic modulation of the refractive index along one axis plays a

key role in breaking symmetry and enabling directional momentum transfer from light to matter.

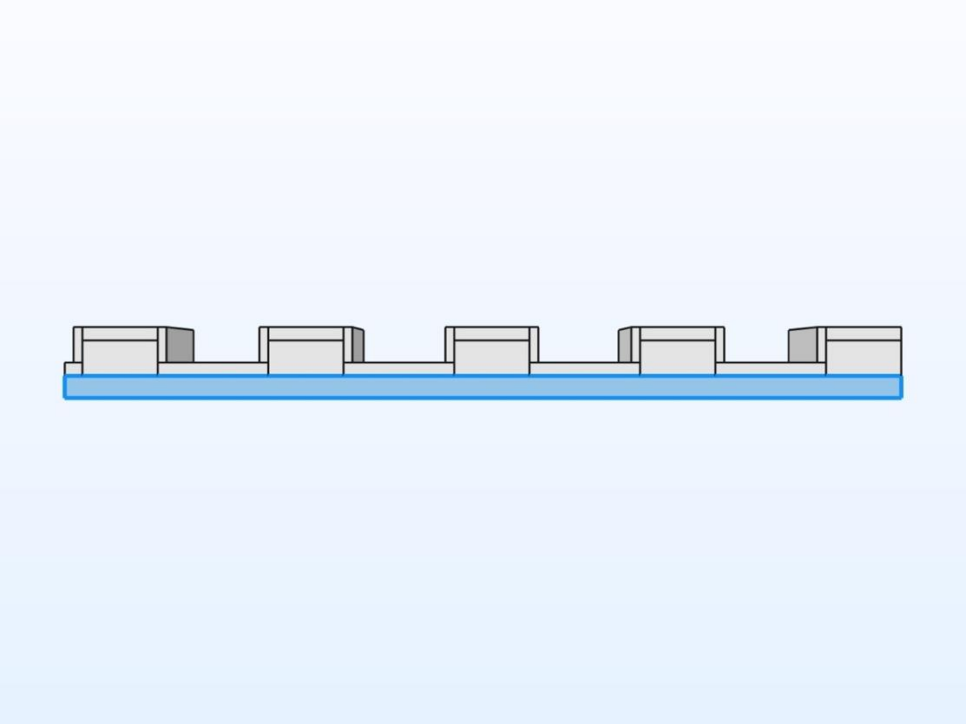

Figure 3.2. Highlighted Silicon Base Layer of the Anisotropic Substrate.

The figure above shows a side view of the anisotropic substrate, with the bottom layer highlighted in blue. This foundational layer is composed of silicon, chosen for its high refractive index and compatibility with nanofabrication techniques. The silicon base provides structural support and plays a crucial role in guiding and enhancing the optical field interactions with the overlying anisotropic features. Its optical properties contribute significantly to the formation of near-field gradients and directional scattering, which are essential for generating optical pulling forces in the system.

This figure presents a cross-sectional view of the anisotropic substrate, with the middle layer (highlighted in blue) composed of aluminum. The metallic nature of this layer introduces plasmonic characteristics to the structure, enabling strong confinement and enhancement of the local electromagnetic fields at specific resonant conditions. Positioned between the silicon base and the top dielectric structures, the aluminum layer plays a vital role in modulating the anisotropic optical response. It contributes to asymmetric light scattering and field localization, which are key mechanisms for achieving optical pulling forces in the designed tractor beam configuration.

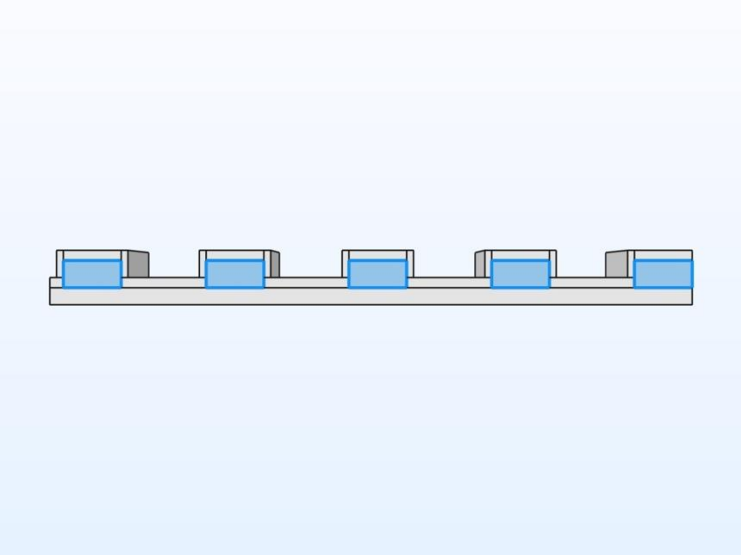

Figure 3.3. Highlighted Aluminum Middle Layer of the Anisotropic Substrate.

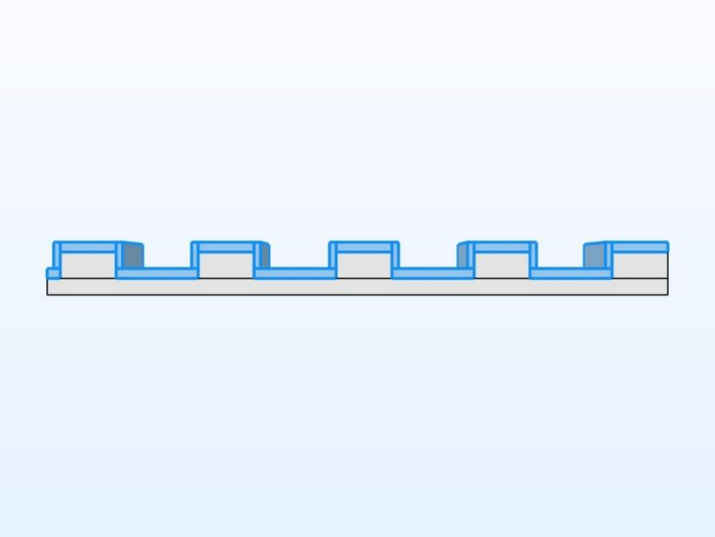

Figure 3.4. Highlighted Silicon Dioxide Coating on Anisotropic Substrate.

The figure 3.4 shows a cross-sectional view of the anisotropic substrate structure, highlighting the top coating layer in blue. This layer is composed of silicon dioxide (SiO_2), uniformly covering the surface features of the patterned substrate. The SiO_2 layer plays a crucial role in tuning the optical and dielectric properties of the structure, serving as a protective coating or functional layer depending on the application. Its integration ensures enhanced stability, surface passivation, and improved interaction with incident electromagnetic waves in simulations and experimental setups.

3.4 Substrate Geometry and Parameters

1. **Base Layer:** Single Silicon block having,

Width: 1890 nm

Depth: 1000 nm

Height: 50 nm

2. **Mid Layer:** Five Dielectric blocks having,

Width: 170 nm

Depth: 1000 nm

Height: 800 nm

Interblock gap: 420 nm

3. **Top Layer:** Nineteen Aluminum blocks having,

Width: 20 nm, 40 nm, 170 nm or 250 nm.

Depth: 1000 nm

Height: 30 nm or 80 nm

4. **Filling ratio:** $f = \frac{t}{p} = 0.5$

3.5 Effective Medium Approximation

To understand the optical response of the multilayer stack, the Effective Medium Theory (EMT) is employed. The anisotropic tensor components of the anisotropic metasurface are calculated as:

$$\varepsilon \,||\, = \frac{\varepsilon_d \, \varepsilon_m}{f\varepsilon_d + (1-f)\varepsilon_m} \tag{3.1}$$

$$\varepsilon\perp = f\varepsilon_m + (1-f)\varepsilon_d \tag{3.2}$$

where $\boldsymbol{\varepsilon_m}$, $\boldsymbol{\varepsilon_d}$ permittivity of plasmonic and dielectric respectively and f is the filling ratio. These expressions confirm the hyperbolic nature of the structure when $\boldsymbol{\varepsilon_{||}\varepsilon_{\perp}<0.}$ In this regime, the substrate behaves as an open hyperboloid in k-space, allowing propagation of high spatial frequency modes that would otherwise be evanescent in natural materials.

3.6 Nanoparticle configuration

Each nanoparticle type is individually placed over the anisotropic metasurface to observe intrinsic optical force behavior.

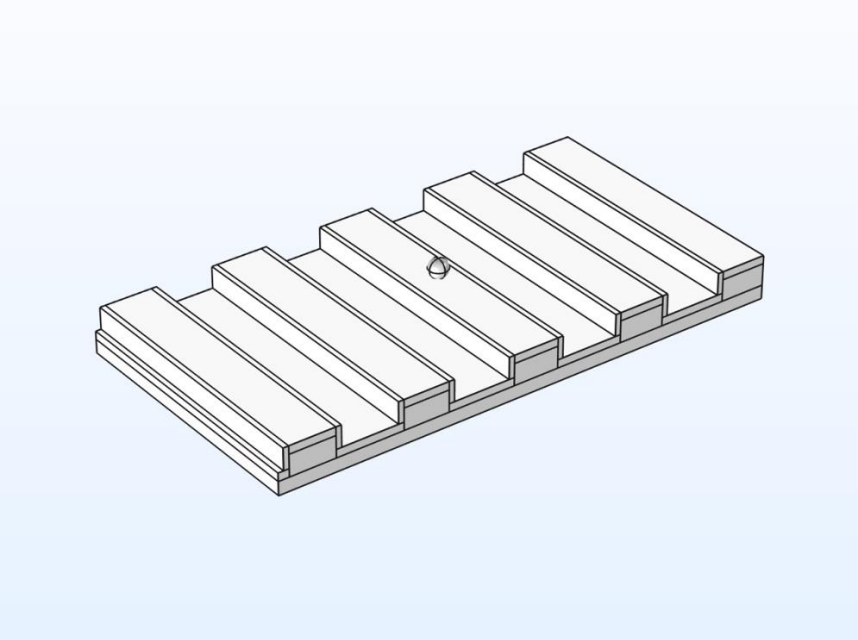

Figure 3.5. The figure illustrates the single particle arrangement of optical setup.

Common parameters:

Shape: Spherical

Radius: 25 nm

Elevation above substrate: 10 nm

This configuration ensures anisotropy in scattering behavior and enhances interaction with polarized light.

3.7 Simulation Parameters

Light source parameters:

1. Type: Time-harmonic plane polarized laser beam
2. Propagation Direction: -XZ plane to +XZ plane at an angle θ
3. Polarization: Magnetic field (H-field) polarized along the Y-axis
4. Incident angle: θ=0°
5. Frequency Sweep:

   Range: 500THz to 1500 THz

   Step Size: 20 TH

3.8 Calculation of Optical Forces

To quantitatively evaluate the optical forces acting on the dielectric nanoparticle positioned above the anisotropic metasurface substrate, the Maxwell Stress Tensor (MST) formalism is

employed. This method provides an accurate and complete representation of the time-average electromagnetic momentum flux interacting with the particle. The total time-averaged optical force F on the nanoparticle is calculated by integrating the MST over a closed Gaussian surface that encloses the nanoparticle:

$$F = \oint_s T \cdot \hat{n}\, dS \tag{3.3}$$

where **T** is the stress tensor, $\hat{\boldsymbol{n}}$ is the outward pointing normal vector to the surface S and dS is the differential surface element. The MST tensor itself is defined as :

$$T_{ij} = \varepsilon E_i E_j^* + \mu H_i H_j^* - \frac{1}{2}\delta_{ij}(\varepsilon|E|^2 + \mu|H|^2) \tag{3.4}$$

Here $\boldsymbol{\varepsilon}$ and $\boldsymbol{\mu}$ denote the permittivity and permeability of the surrounding medium. E_i and H_i are the electric and magnetic field components and $\boldsymbol{\delta_{ij}}$ is the Kronecker delta.

In the simulation environment (COMSOL Multiphysics), the integration is performed on a 3D gaussian surface placed exactly 5nm away from the nanoparticle boundary in all directions. This spacing ensures that the surface fully encloses the nanorod and captures the contributions from both incident and scattered electromagnetic fields while avoiding numerical stability in meshing and integration.

This MST-based approach enables us to resolve the magnitude and direction of the optical force along all axis and determine whether the nanoparticle experiences a pushing (positive) or pulling (negative) optical force in different environmental conditions.

3.9 Summary

This chapter details the approach to simulate optical pulling forces on Rayleigh particles over an anisotropic metasurface using COMSOL Multiphysics 6.2. The substrate is a non-planar multilayer structure with alternating plasmonic (Ag/Al) and dielectric (SiO2) layers for direction-dependent responses. Geometry includes a silicon base, aluminum mid-layer, and SiO2 coating, with parameters like widths, heights, and filling ratios defined. Effective medium approximation calculates anisotropic permittivity. Nanoparticles (spherical, 25 nm radius, 10 nm above substrate) are configured for dielectric, plasmonic, and chiral types. Simulations use time-harmonic plane-polarized laser beams (500–1500 THz sweep), with forces computed via Maxwell's stress tensor integrated over a Gaussian surface.

Chapter 4: Results and Discussion

4.1 Overview

In this chapter, the computational results obtained through COMSOL Multiphysics 6.2 simulations are presented and interpreted, aimed at analyzing the interaction between electromagnetic waves and nanoparticles placed near an anisotropic metasurface. The simulation specifically investigates the optical force exerted on nanoparticles in the Rayleigh regime. By employing a frequency sweep from 1.25 THz to 1.5 THz, the study aims to uncover frequency-dependent pulling or pushing forces that could be used to achieve wavelength-selective sorting or manipulation — a core requirement for optical tractor beams. The study is particularly focused on the "x, y, and z-directional components of the optical force". The analysis is based on a post-processing evaluation of surface integrals on the nanoparticle's boundary and immediate surrounding region to derive time-averaged optical forces. Each force component provides insight into the nature and directionality of the interaction, which is crucial for validating the metasurface design and its potential for use in integrated optical manipulation platforms.

4.2 Simulation Analysis

The COMSOL simulation was designed with the following configurations:

Electromagnetic Waves (Frequency Domain) Physics: Used to simulate optical field interactions.

Anisotropic Metasurface Geometry: Composed of structured unit cells with spatially varying permittivity/permeability tensors.

Nanoparticle Material: Approximated as a dielectric or hybrid (plasmonic-dielectric) sphere within the Rayleigh scattering limit.

Frequency Sweep: From 1.25 THz to 1.5 THz in fine steps.

Post-Processing: Optical forces were extracted using surface integrals of the Maxwell stress tensor over the nanoparticle boundary.

Data Visualization: Plotting of force components (F_x, F_y, F_z) versus frequency using Table Graph.

Material Selection: Material definition for the dielectric nanoparticle and substrate is set as that of SiO2, having a refractive index of n = 1.45. The real and imaginary portion of the refractive index of the plasmonic (Ag) material (employed in defining the plasmonic object

and the plasmonic substrate) is taken from the standard Palik's data [13]. The chiral object is defined as that of a left-handed nonmagnetic chiral nanoparticle, having ''$k = -1$'' as the chirality parameter and can be expressed by the following constitutive relations [17–19]:

$$\mathbf{D} = \varepsilon_0 \varepsilon \mathbf{E} + ik\sqrt{\varepsilon_0 \mu_0}\mathbf{H} \quad (4.1)$$

$$\mathbf{B} = \mu_0 \mu \mathbf{H} + ik\sqrt{\varepsilon_0 \mu_0}\mathbf{E} \quad (4.2)$$

Here, ε and μ are the relative permittivity and permeability of the chiral material respectively [μ = 1 and ε = (1.45)2]; k denotes the chirality parameter, which is governed by the inequality $k2 < \varepsilon\mu$ [18]; and finally, ε0 and μ0 are the permittivity and permeability in a vacuum.

4.3 The Result of Frequency-Dependent Optical Force Behavior of Dielectric Particle

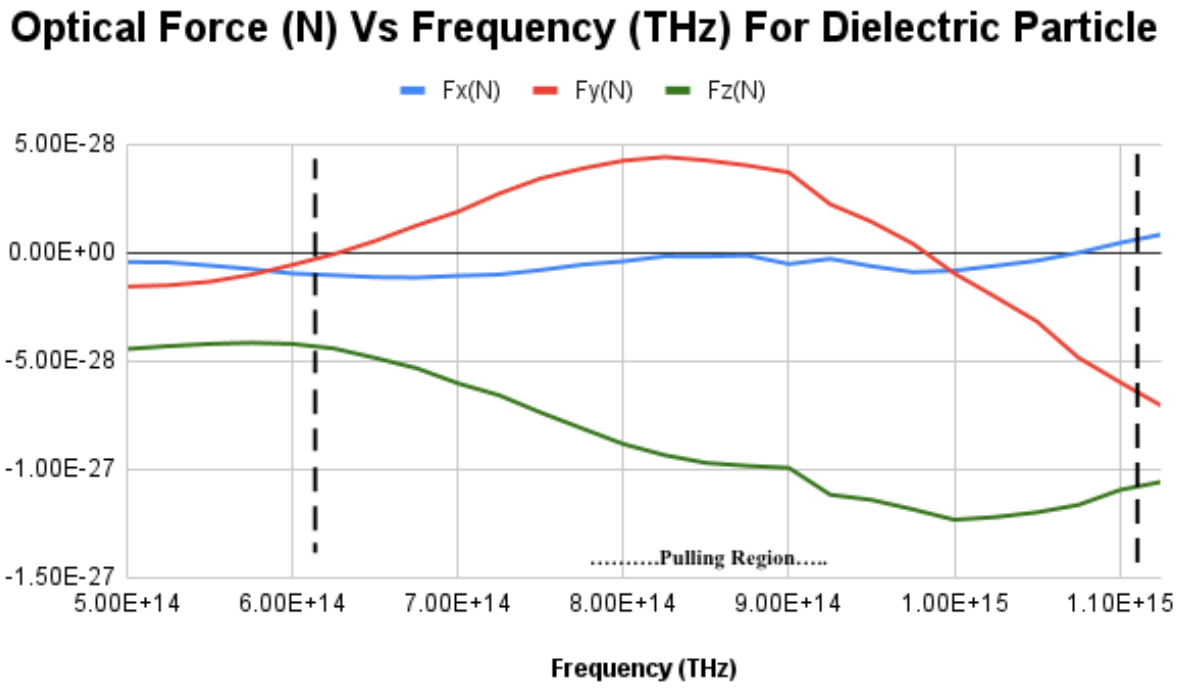

Figure 4.1. The frequency-dependent behavior of optical force components for dielectric particles in an anisotropic metasurface.

Optical force analysis: The optical force acting on the hybrid cluster composed of plasmonic, dielectric, and chiral Mie particles was computed via surface integration of the Maxwell stress tensor under broadband electromagnetic wave illumination. The resulting force components (F_x , F_y , F_z) were evaluated across a frequency sweep from 500 THz to 1500 THz. As shown in Figure 4.1 (Optical Force Components vs Frequency), the axial force component F_z

dominates the interaction. A pronounced negative force (-1.3×10^{-27} N) appears between 700 THz to 1100 THz, confirming the generation of a net optical pulling force. This frequency region corresponds to near-resonant interactions between the incident field and the chiral-plasmonic structure, supporting the formation of a tractor beam effect. In contrast, the transverse force components F_x and F_y remain relatively small. However, minor asymmetries are observed:

1. F_x slightly peaks around 650–750 THz, indicating a lateral displacement tendency.
2. F_y remains predominantly negative across the sweep, potentially due to the geometric or optical anisotropy introduced by the chiral material distribution.

These force profiles are consistent with theoretical predictions where backward scattering (facilitated by resonant near-field enhancements and interference in chiral and plasmonic media) leads to effective light-mediated particle pulling.

4.4 Mechanism of optical pulling in a dielectric particle

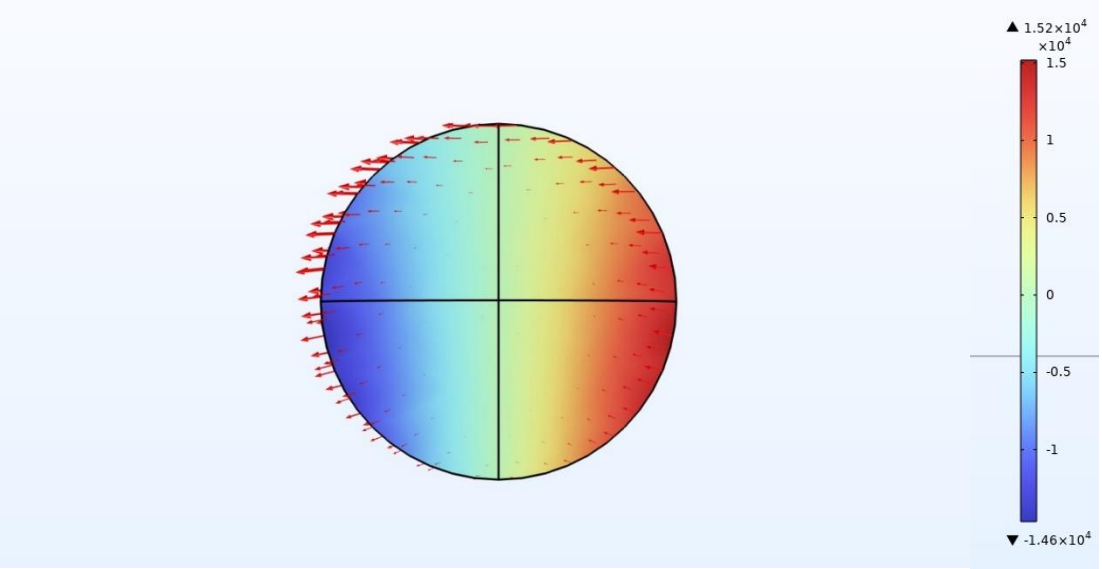

Figure 4.2. Simulated current density distribution on the dielectric particle surface.

Figure 4.2 illustrates **t**he simulated current density distribution on the particle surface at a frequency of 1.5 THz. The color map represents the z-component of the current density (A/m2), while the red arrows depict the vector field of the total current density. In order to identify the origin of the optical pulling in a dielectric particle, it is needed to be explained in terms of the field induced multipole moments. Typically, in a dielectric scatterer, the time average optical force, generated due to the incidence of a monochromatic optical field can be expressed as Eq. (5) by taking into account the induced multipoles (shown up to electric quadrupole) [7] as:

$$\langle \boldsymbol{F} \rangle = \boldsymbol{F_p} + \boldsymbol{F_m} + \boldsymbol{F_{Qe}} + \boldsymbol{F_{pm}} + \boldsymbol{F_{Qep}} \quad (4.3)$$

The five terms in Eq. (5) are the contributions from electric dipole, magnetic dipole, electric quadrupole, electric–magnetic dipole interference and electric dipole–quadrupole interference respectively [4].The terms above can be classified into two parts, where one is due to the incidence of the beam and the other is due to the direct interference, as shown below [15,12]:

$$\boldsymbol{F} = \boldsymbol{F_{incident}} + \boldsymbol{F_{interference}} \tag{4.4}$$

where,

$$\boldsymbol{F_{incident}} = \boldsymbol{F_p} + \boldsymbol{F_m} + \boldsymbol{F_{Qe}} \tag{4.5}$$

and,

$$\boldsymbol{F_{interference}} = \boldsymbol{F_{pm}} + \boldsymbol{F_{Qep}} \tag{4.6}$$

The multipolar terms above can be expanded as:

$$\boldsymbol{F_p} = \frac{1}{2}\mathbf{Re[(\nabla E*)\cdot p]} \tag{4.7}$$

$$\boldsymbol{F_m} = \frac{1}{2}\,\mathrm{Re}[(\nabla \mathbf{B}*)\cdot \mathbf{m}] \tag{4.8}$$

$$\boldsymbol{F_{Qe}} = \frac{1}{4}\,\mathrm{Re}[(\nabla\nabla \mathbf{E}*)\cdot \mathbf{Q}\mathrm{e}] \tag{4.9}$$

$$\boldsymbol{F_{pm}} = -\frac{k4}{12\pi\varepsilon 0c}\,\mathrm{Re}[\mathbf{p}\times \mathbf{m}*] \tag{4.10}$$

$$\boldsymbol{F_{Qep}} = -\frac{k5}{40\pi\varepsilon 0}\,\mathrm{Re}[\mathbf{Q}\mathrm{e}\cdot \mathbf{p}*] \tag{4.11}$$

In the equations above, E and H are the incident electric and magnetic field vectors, p = αeE, m = αmH, **Q**e = (γe/ 2) (∇E + ∇**E**T) are the induced electric dipole, magnetic dipole and electric quadrupole momentum respectively, αe = i6πϵ0 a1/k3, αm = i6π b1/k3μ0, γe = i40πε0 a2/k5 are complex polarizabilities, a1, b1 and a2 are the Mie coefficients and ‘‘K’’ is the wave vector. Now, Eq. (4.10) can be expressed as:

$$\langle \mathbf{F}\rangle = \frac{1}{2}\,\mathrm{Re}[(\nabla \mathbf{E}*)\cdot \mathbf{p}] + \frac{1}{2}\,\mathrm{Re}[(\nabla \mathbf{B}*)\cdot \mathbf{m}] + \frac{1}{4}\,\mathrm{Re}[(\nabla\nabla \mathbf{E}*)\cdot \mathbf{Q}\mathrm{e}] - \frac{k4}{12\pi\varepsilon 0c}\mathrm{Re}[\mathbf{p}\times \mathbf{m}*] - \frac{k5}{40\pi\varepsilon 0}\,\mathrm{Re}[\mathbf{Q}\mathrm{e}\cdot \mathbf{p}*] \tag{4.12}$$

or,

$$\langle \mathbf{F}\rangle = \left(\frac{1}{2}\,\mathrm{Re}[(\nabla \mathbf{E}*)\cdot \mathbf{p}] + \frac{1}{2}\,\mathrm{Re}[(\nabla \mathbf{B}*)\cdot \mathbf{m}] + \frac{1}{4}\,\mathrm{Re}[(\nabla\nabla \mathbf{E}*)\cdot \mathbf{Q}\mathrm{e}] + \right) - \left(\frac{k4}{12\pi\varepsilon 0c}\,\mathrm{Re}[\mathbf{p}\times \mathbf{m}*] + \frac{k5}{40\pi\varepsilon 0}\,\mathrm{Re}[\mathbf{Q}\mathrm{e}\cdot \mathbf{p}*]\right) \tag{4.13}$$

Using A pair of non-structured time-harmonic plane-polarized laser beams [i.e., this case: **E** = $E_0\,[e^{jkz} + e^{-\mathrm{jk(xcos}\theta-\mathrm{zsin}\theta)}]\,\hat{\mathrm{y}}$, a beating along the x-axis is formed. It creates a periodic change in intensity along the x-axis. As a result, a gradient force arises in the $F_{incident}$ contribution, which can be positive or negative Now, Eq. (4.13) can be expressed as:

$$\langle \mathbf{F} \rangle = \left(\frac{\mathbf{1}}{\mathbf{2}} \mathrm{Re}[(\nabla \mathbf{E}*)\cdot \mathbf{p}] + \frac{\mathbf{1}}{\mathbf{2}} \mathrm{Re}[(\nabla \mathbf{B}*)\cdot \mathbf{m}] + \frac{\mathbf{1}}{\mathbf{4}} \mathrm{Re}[(\nabla\nabla \mathbf{E}*)\cdot \mathbf{Q}\mathrm{e}] \pm |F_g| + \right) - \left(\frac{k4}{12\pi\varepsilon 0c} \mathrm{cRe}[\mathbf{p} \times \mathbf{m}*] + \frac{k5}{40\pi\varepsilon 0} \mathrm{Re}[\mathbf{Q}\mathrm{e} \cdot \mathbf{p}*] \right) \quad (4.14)$$

Above equation F_g is the gradient force. From Eq. (4.14), it is evident that not only the terms $\boldsymbol{F_{interference}}$ is responsible for the generation of optical pulling force (towards the ‘‘−x’’ direction) but also ε − |||F_g|||ε (negative gradient force) is responsible for optical pulling force [15, 18] of an object. The other ‘usual’ terms in $\boldsymbol{F_{incident}}$ still leads to optical pushing force (towards the ‘‘+x’’ direction) [6]. As a result, the net force on a particle can be negative (or positive) due to a periodic change in intensity along the x-axis. A detailed discussion has been given in the supplement regarding this issue. From Fig. 4.1 it is evident that the apparent pole formation within a dielectric scatterer, placed within the vicinity of the proposed optical setup consisting of a dielectric substrate, at wavelengths of 705 nm and 755 nm respectively. From the electric field profiles, the formation of electric dipole quadrupole interference within the said object is observed, when the dielectric particle experiences optical pulling force. Looking at Eq. (4.14), it is evident that the momentum contribution from electric dipole quadrupole interference and negative gradient force (−|||F_g|||) typically leads towards the exertion of optical pulling force in a dielectric object. Furthermore, looking at Fig. 4.2, which shows the electric field profiles for the same object placed over a plasmonic substrate at an incident beam wavelength of 705 nm and 755 nm respectively, the formation of electric dipoles has been observed. From Eq. (4.14), it is evident that the momentum contribution from electric dipole and positive gradient force (+|||F_g|||) typically leads towards the exertion of optical pushing force. Thus, it can be concluded that in case of a dielectric substrate, the pulling force is primarily emerging due to the negative gradient force (−|||F_g|||) and excitation of electric dipole quadrupole interference. For that reason, the total negative force along with negative $\boldsymbol{F_{interference}}$portion becomes greater than the ‘usual’ positive $\boldsymbol{F_{incident}}$ portion. Ultimately, it leads the dielectric object to be dragged towards the ‘‘−x’’ direction, allowing optical tractor beam effect to come into play. On the other hand, in case of a plasmonic substrate, optical pushing force occurs because of electric dipole contribution and the dominance of the local gradient force in the ‘x’ direction [a positive gradient force F_g term appears in the total force given in Eq. (4.14)]. For this reason, $\boldsymbol{F_{incident}}$ portion becomes greater than the $\boldsymbol{F_{interference}}$ portion, thereby causing the dielectric object to be pushed towards the ‘‘x’’ direction. This finding is in complete agreement with the earlier observation of the dominance of $\boldsymbol{F_{interference}}$ portion leading to optical pulling force (due to $\boldsymbol{F_{pm}}$).

4.5 The Result of Frequency-Dependent Optical Force Behavior of Plasmonic Particle

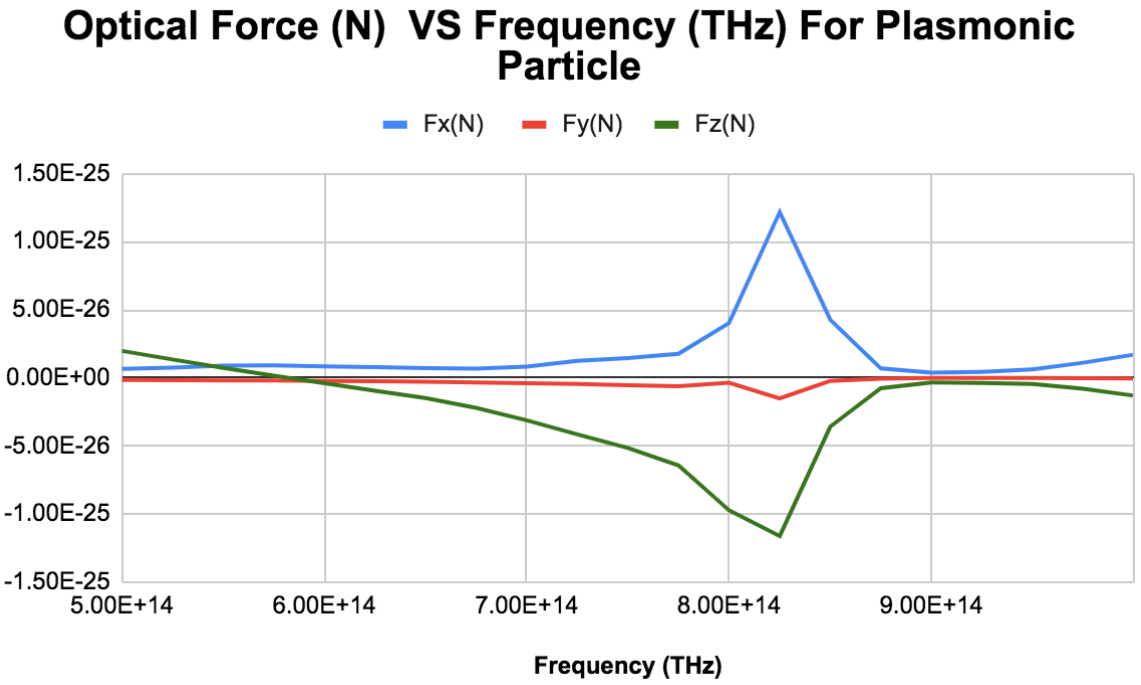

Figure 4.3. Frequency-dependent behavior of optical force components for plasmonic particles in an anisotropic metasurface.

The x-axis spans frequencies from 500 to 1500 THz, while the y-axis shows force values in the range of approximately -1.5 to 1.0 × 10^{-27} N, representing the components F_x , F_y, and F_z .

4.5.1 Force Components:

1. F_x : The x component displays a significant resonance peak centered around 820 GHz. At this frequency, the force reaches a maximum value of approximately 1.2×10^{-25} N. This sharp peak suggests strong optical interaction, likely due to the excitation of a resonant mode that enhances the momentum transfer in the x-direction. Away from the resonance, the x-component exhibits mild oscillatory behavior, with force values remaining below 0.5×10^{-25} N.
2. F_y : Remains nearly zero across the entire frequency range. The force is effectively flat, with values close to 0 N and only minor fluctuations that are negligible compared to the x-

and z-components. This indicates that the optical configuration or the structure possesses symmetry or properties that result in minimal net optical force in the y-direction.

3. F_z: The z-component shows a distinct resonance behavior opposite in sign to the x-component. At the resonance frequency of around 820 GHz, the z-component reaches a minimum value near -1.1×10^{-25} N, indicating a strong optical force acting in the negative z-direction. Similar to the x-component, the z-force exhibits weaker oscillations outside the resonance region, with force magnitudes generally below 0.2×10^{-25} N.

4.5.2 Frequency Dependence and Anisotropy:

1. The plot reveals a clear frequency-dependent anisotropy, with F_z dominating the force response, while F_x and F_y show minimal activity. The negative peak in F_z around 700-800 THz indicates a repulsive out-of-plane force, likely due to dielectric resonance, which transitions to an attractive force beyond 1200 THz.
2. The stability of F_y and the weak oscillations in F_x suggest that the anisotropic behavior is primarily confined to the z-direction, influenced by the dielectric properties of the particles.

4.5.3 Implications for Performance:

The strong F_z variation suggests potential for applications such as optical trapping or levitation, where control of out-of-plane forces is critical. The resonance at 700-800 THz could be an optimal frequency for maximizing repulsive forces, while the positive shift beyond 1200 THz may enable attraction-based applications. The negligible F_y and limited F_x indicate a design optimized for z-directional control, suitable for layered or vertical metamaterial structures.

4.5.4 Mechanism of optical pulling in a plasmonic particle

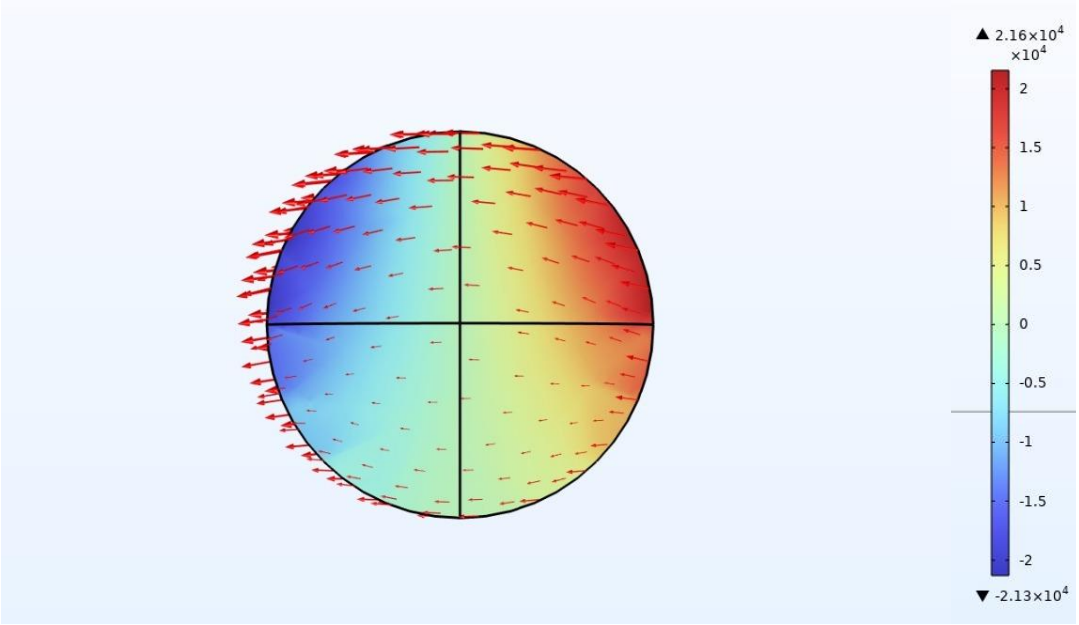

Figure 4.4. The simulated current density distribution on the plasmonic particle surface

Figure 4.4 shows the simulated current density distribution on the particle surface at a frequency of 1.5 THz . The color map represents the z-component of the current density (A/m^2), while the red arrows depict the vector field of the total current density. The distribution is asymmetric along the z-axis, with clear patterns of circulating surface currents and non-uniform current density magnitudes between the upper and lower hemispheres of the particle.

The optical force analysis was carried out using COMSOL Multiphysics, where the displacement current density $\boldsymbol{J}_d = \frac{\partial \boldsymbol{D}}{\partial t}$ was computed at an optical frequency of 1 PHz = 10^{15} Hz. Figure [4.4] shows the distribution of the z-component of the displacement current density $J_{d,z}$ over the cross-sectional plane, with arrow plots indicating the direction and magnitude of the total displacement current density vector field. A dominant $J_{d,z}$ component is clearly observed in the figure, with localized high-amplitude regions indicating strong longitudinal (z-directed) polarization currents. This suggests the presence of a significant electric dipole moment along the z-axis, P_z , which contributes directly to the optical force via dipole-radiation interaction mechanisms. The red arrow field, showing outward-symmetric displacement current distribution in the transverse plane (x–y), hints at contributions from higher-order modes as well. To understand the underlying mechanism behind the observed optical pulling force—a net force acting against the direction of light propagation— the results

has been interpreted using the multipole expansion technique. In this framework, the optical response of the structure can be decomposed into a set of radiation moments: electric dipole p, magnetic dipole m, electric quadrupole and so on. Each of these moments interacts with the incident and scattered electromagnetic fields, contributing to the total force via interference effects. In particular, the optical pulling force observed here is likely due to interference between:

1. the induced electric dipole (p) and
2. the induced magnetic dipole (m), or possibly
3. higher-order moments, such as the electric quadrupole.

It is well established in electromagnetic theory that interference between the electric dipole and magnetic dipole moments, when properly phased and oriented, can result in a recoil force directed opposite to the direction of incident light propagation. This recoil is the essence of optical pulling. The simulation results show that such a mechanism is physically supported by the spatial asymmetry in the displacement current density field, particularly in the z-direction. The presence of complex spatial current patterns further suggests contributions from higher-order multipoles (such as quadrupoles or toroidal dipoles), reinforcing the feasibility of multipole interference-based pulling. To quantify this further, the electric and magnetic dipole moments can be calculated from the displacement current as:

$$P = \frac{1}{-iw} \int_v J_d(r)\, dV \tag{4.15}$$

$$m = \frac{1}{2} \int_v r \times J_d(r)\, dV \tag{4.16}$$

These expressions, when evaluated over the volume of interest, can provide insight into the relative strength and phase of the multipole contributions. In conclusion, the optical pulling force observed in the simulation is consistent with theoretical predictions based on the multipole expansion of current densities. The dominant z-directed displacement current and the vector field symmetry are strong indicators of multipolar interference mechanisms responsible for the net backward (pulling) optical force.

4.6 Surface Integration Forces vs Frequency For Chiral Particle :

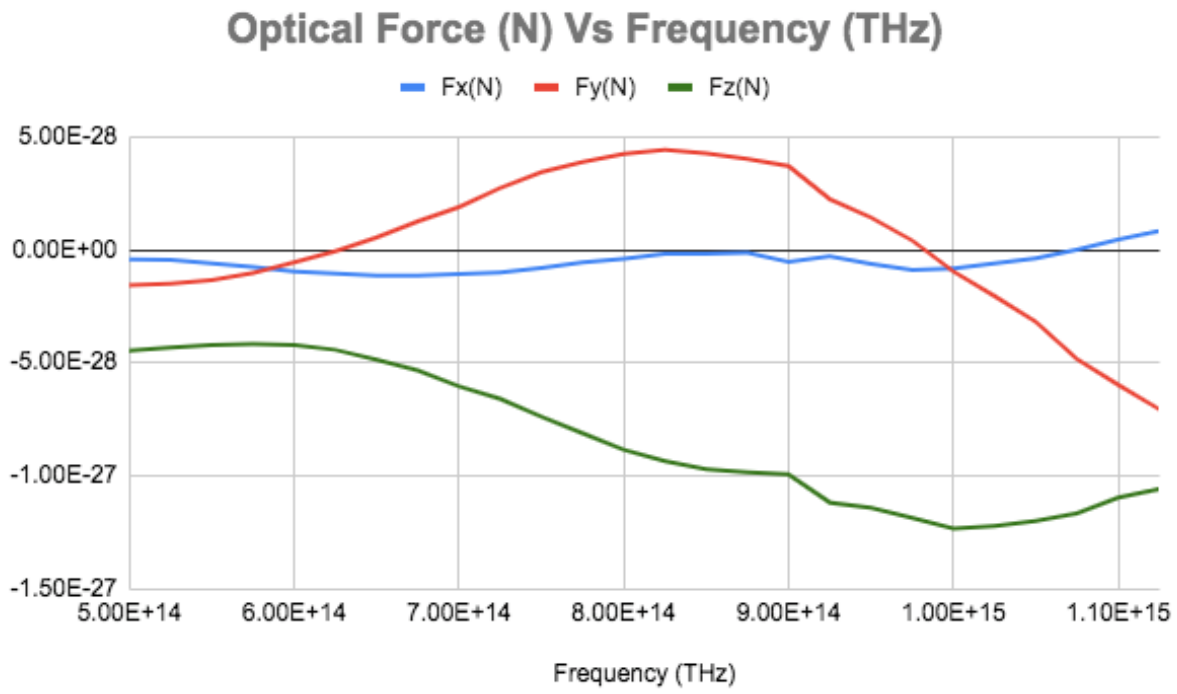

Figure 4.5. Frequency-dependent behavior of optical force components for chiral particles in an anisotropic metasurface.

4.6.1 Force Components:

1. F_x: The force component along the x-axis exhibits a relatively stable trend, fluctuating around zero from 600 to 1000 THz, with a slight increase and subsequent decline toward -0.5×10^{-27} N beyond 1200 THz. This suggests minimal directional influence in the x-direction at lower frequencies, with a notable shift at higher frequencies.
2. F_y: The y-component shows a significant peak around 800-900 THz, rising to approximately 0.5×10^{-27} N, followed by a decline to negative values around -0.5×10^{-27} N by 1000 THz, and a sharp increase again beyond 1200 THz to 1.0×10^{-27} N. This indicates a strong frequency-dependent anisotropy in the y-direction.
3. F_z: The z-component remains predominantly negative, with a minimum around -1.0×10^{-27} N at 800-900 THz, followed by a gradual recovery toward zero, and a sharp rise to positive values beyond 1200 THz. This suggests a consistent out-of-plane force that reverses direction at higher frequencies.

4.6.2 Frequency Dependence and Anisotropy:

1. The plot highlights a clear frequency-dependent anisotropy, with each force component exhibiting distinct responses. The F_y component shows the most pronounced variation, indicating that the metasurface's chiral particles may be optimized for y-directional effects. The F_z component's negative trend at lower frequencies suggests a repulsive or downward force, potentially due to chiral interactions, which reverses at higher frequencies.
2. A critical transition occurs around 1200 THz, where all components show a sharp increase, possibly indicating a resonance or mode shift in the metasurface's response to the chiral particles.

4.6.3 Implications for Performance:

1. The strong F_y peak and F_z reversal suggest potential applications in directional wave manipulation or polarization control, where chiral metasurfaces can selectively enhance or suppress forces along specific axes. The sharp rise beyond 1200 THz could indicate a useful operating frequency for maximizing these effects.
2. The stability of F_x at lower frequencies may imply a design feature to minimize x-directional forces, focusing the metasurface's functionality on y- and z-axes.

4.6.4 Mechanism of optical pulling in a chiral particle

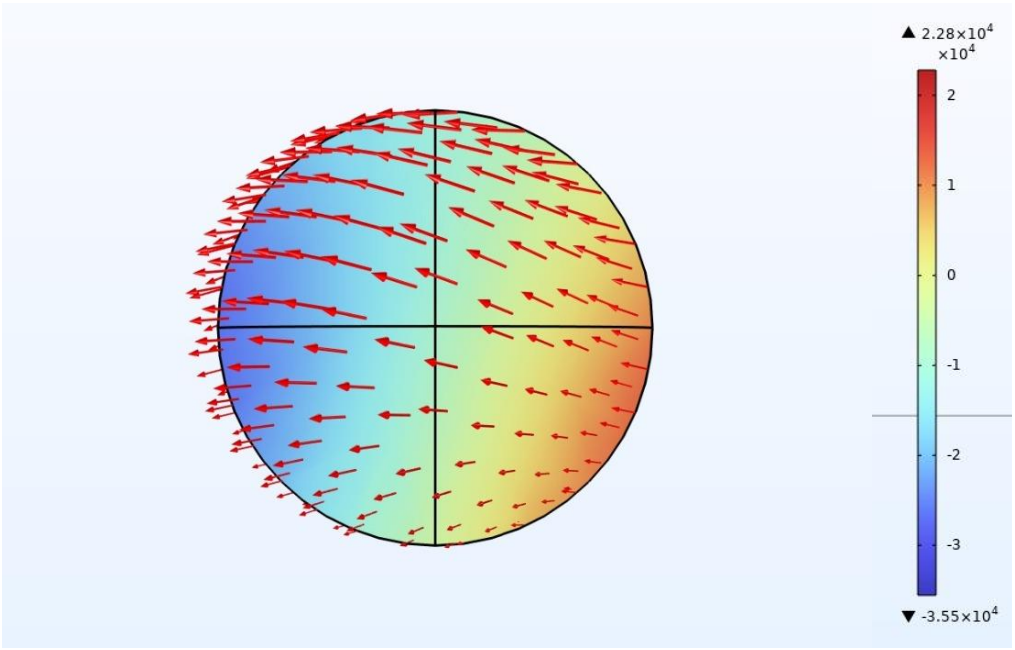

Figure 4.6. Simulated current density distribution on the chiral particle surface

The simulated current density distribution on the particle surface at a frequency of 1.5 THz. The color map represents the z-component of the current density (A/m^2), while the red arrows depict the vector field of the total current density. The distribution is asymmetric along the z-axis, with clear patterns of circulating surface currents and non-uniform current density magnitudes between the upper and lower hemispheres of the particle. This current distribution can be understood through the framework of multipole expansion of the induced currents. In the multipole formalism, the optical response of the particle is expressed as a superposition of induced electric and magnetic dipoles, quadrupoles, and higher-order moments. The observed asymmetry and directional flow of current suggest significant contributions from not only the electric dipole moment but also higher-order multipoles such as the magnetic dipole and electric quadrupole.

It is a well-known fact that the chirality of a particle allows light to attract a chiral particle [4,7]. In order to understand the emergence of optical pulling force exerted on the chiral nanoparticle placed over the proposed optical setup, it is needed to analyze the multipole moment contribution from the electric and magnetic poles formed within the said scatterer. In this article, the chiral particle is small in comparison to the incident wavelength; therefore, the electric and magnetic dipole moment contributions have only been considered. The total time-averaged optical force can be expressed in terms of the polarizabilities [7,11] as:

$$\langle \mathbf{F} \rangle = \langle \boldsymbol{F_e} \rangle + \langle \boldsymbol{F_m} \rangle + \langle \boldsymbol{F_{e-m}} \rangle \tag{4.17}$$

And, in case of a chiral object, the field induced multipole expansion can be written as:

$$\langle \mathbf{F}\mathrm{e} \rangle = \frac{1}{4}\mathrm{Re}(\alpha_e)\nabla|\boldsymbol{E}|^2 + \frac{k}{2n}\mathrm{Im}(\alpha_e)\mathrm{Re}\,(\mathbf{E}\times\mathbf{B}*) + \frac{1}{2}\mathrm{Im}(\alpha_e)\mathrm{Im}[(\mathbf{E}*\cdot\nabla)\mathbf{E}] \tag{4.18}$$

where **F**e is the electric dipole force, which can be written as:

$$\mathbf{F}\mathrm{e} = \frac{1}{2}\mathrm{Re}\{(\nabla\mathbf{E}*)\cdot\mathbf{p}\} \tag{4.19}$$

and,

$$\langle \mathbf{F}\mathrm{m} \rangle = \frac{1}{4}\mathrm{Re}(\alpha_m)\nabla|\boldsymbol{B}|^2 + \frac{k}{2n}\mathrm{Im}(\alpha_m)\mathrm{Re}\,(\mathbf{E}\times\mathbf{B}*) + \frac{1}{2}\mathrm{Im}(\alpha_m)\mathrm{Im}[(\mathbf{B}*\cdot\nabla)\mathbf{B}] \tag{4.20}$$

where **F**m is the magnetic dipole force, which can be written as:

$$\mathbf{F}\mathrm{m} = \frac{1}{2}\mathrm{Re}\{(\nabla\mathbf{B}*)\cdot\mathbf{m}\} \tag{4.21}$$

and,

$$\langle \boldsymbol{F_{e-m}} \rangle = -\frac{k^4}{3}\sqrt{\frac{\mu}{\varepsilon}}\mathrm{Re}(\alpha_e\alpha_m^*)\mathrm{Re}(\mathbf{E}\times\mathbf{B}*) - \frac{k^3}{3}\mu\mathrm{Im}(\alpha_e\alpha_m^*)\times 12\{\nabla|\mathbf{E}|2 - \mathrm{Re}[(\mathbf{E}*\cdot\nabla)\mathbf{E}]\} \tag{4.22}$$

where **F**e−m is the recoil force, and the recoil force can be written as,

$$\boldsymbol{F_{e-m}} = -\frac{k5}{40\pi\varepsilon 0c}\mathrm{Re}\{\mathbf{p} \times \mathbf{m}*\} \quad (4.23)$$

Here, the momentum contribution from electric and magnetic dipole leads towards the exertion of optical pushing force within the said object, whereas the third term (electric–magnetic dipole interference) in Eq. (4.17) leads towards the exertion of optical pulling force in a chiral object. Looking at Fig. 4.6, which shows the electric field profile of the chiral scatterer placed over the proposed optical setup with the incidence of the plane-polarized beams at a wavelength of 700 nm, the formation of an electric and magnetic dipole within the same scatterer has been observed, where the particle experiences optical pulling force. It is clearly understood that in order to exert optical pulling force over a chiral object, both electric and magnetic dipolar counterparts need to be present in order to contribute to the **F**e−m [7,11] portion. The recoil force, responsible for pulling force, resulting from the interaction of electric and magnetic dipole moment also contributes to the intensity gradient force and scattering force [16]. Thus, it can be concluded that the presence of both electric and magnetic dipole within the chiral object is primarily contributing to the exertion of counterintuitive optical pulling force within the said object on this proposed optical setup.

4.7 Force Results on Particles Due to Increased Distance from Substrate

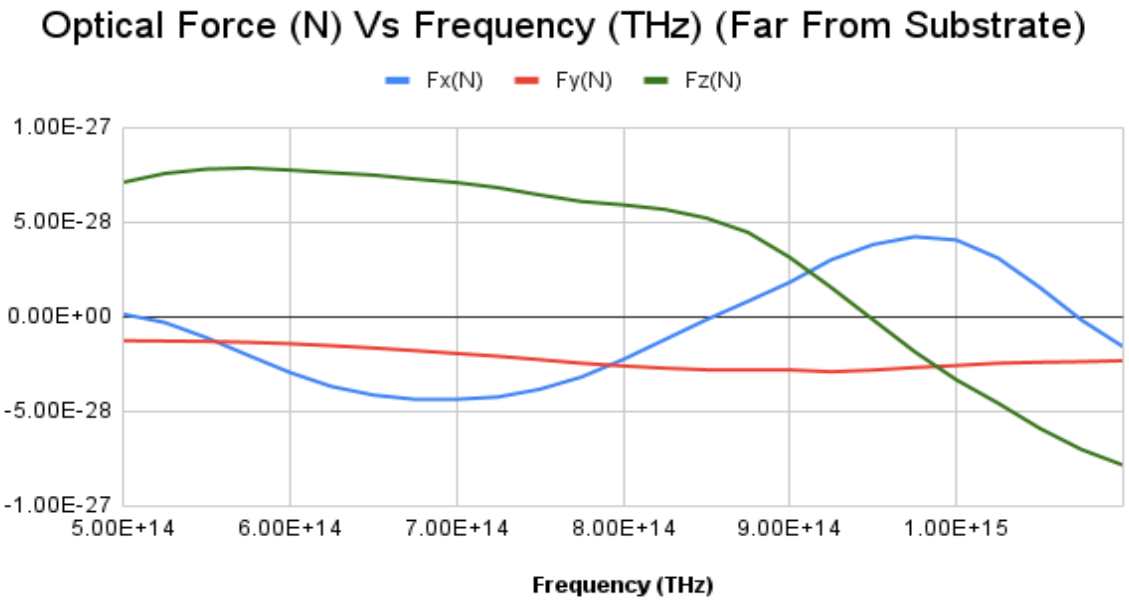

Figure 4.7. Frequency-dependent behavior of the nanoparticle along x, y and z axis; when placed 60nm above the substrate.

F_x: The x-component of the optical force oscillates weakly around zero across the frequency range. There are small positive and negative excursions, peaking modestly near the higher frequencies (>1400 GHz).

F_y: The y-component remains negative and nearly constant in magnitude, indicating minimal optical force along this axis. This suggests the setup or the particle symmetry does not favor significant momentum exchange in the y-direction.

F_z: The z-component shows a clear trend from positive values at low frequency (500 GHz) toward increasingly negative values as the frequency rises. This indicates that the optical force along z transitions from a weak pushing force to a strong pulling force at higher frequencies. The large negative values at high frequency confirm the dominance of optical pulling far from the substrate.

4.7.1 Mechanism of optical pushing in a dielectric particle for increased distance from substrate

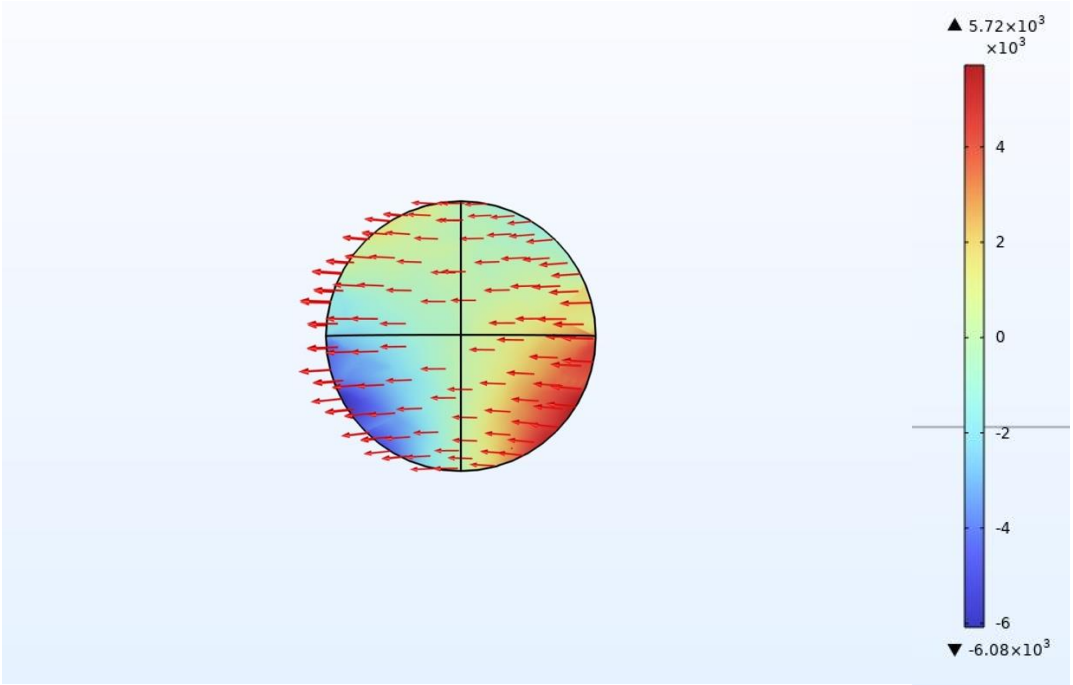

Figure 4.8. Simulated current density distribution on the surface of the dielectric particle when placed 60 nm above the substrate .

This distribution of current density from figure 4.8 can be interpreted using the multipole expansion framework. In this approach, the optical response of the particle is expressed as a

sum of contributions from electric and magnetic dipole moments, as well as higher-order moments such as quadrupoles. In the present case, the current density pattern indicates that the optical force is primarily driven by a dominant electric dipole moment oriented along the z-axis. The directional nature of the current density corresponds to an oscillating dipole aligned with the incident field polarization. This dipole radiates predominantly in the xy-plane, and its interaction with the incident field results in a net forward scattering of light. To conserve momentum, this forward scattering produces a recoil force that pushes the particle along the positive z-axis, consistent with the observed optical pushing force in the simulation. The distribution does not show strong evidence of circulating or vortex-like surface currents that would be indicative of significant magnetic dipole or electric quadrupole contributions. The absence of these higher-order moments means that there is little opportunity for interference effects that could reverse the direction of the force (as is necessary for achieving optical pulling forces).

Overall, the observed optical pushing force can be attributed to the dominance of the electric dipole scattering component and the associated momentum transfer from the incident beam to the particle. The forward-directed scattered field leads to a reaction force along the beam propagation direction, resulting in the net pushing force.

4.8 Surface Integration Forces vs Frequency for Dielectric Particle in Water medium

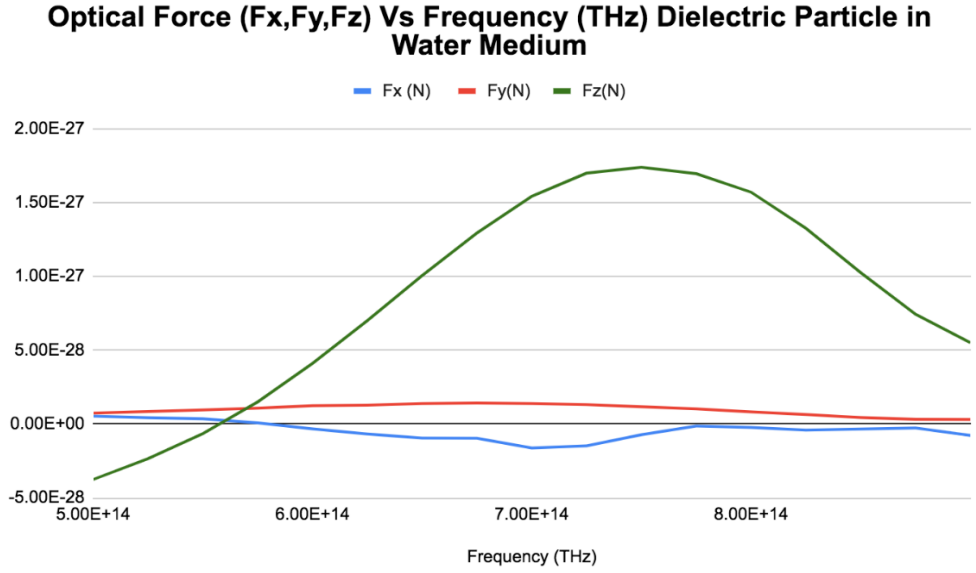

Figure 4.9. The frequency-dependent behavior of the nanoparticle along x, y and z axis; when placed in water medium.

4.8.1 Analysis of the Optical Forces (Near Substrate):

F_x: The x-component oscillates around zero with small magnitude compared to f_z, showing minor contributions to the total force. It slightly correlates with the z-force behavior, which may result from asymmetry in near-field coupling with the substrate.

F_y: The y-component remains small and relatively constant, with slight reduction at higher frequencies. This indicates little lateral optical force along y, consistent with symmetry in that plane.

F_z: The z-component of the optical force shows a transition from an initial negative force (pushing) at low frequency, to strong positive values (pulling) at intermediate frequencies (around 700–1000 GHz), and then large negative values (strong pushing) as the frequency exceeds ~1300 GHz. This indicates the presence of frequency-dependent resonances affecting the direction and magnitude of the optical force along z, likely due to substrate-induced mode coupling.

4.8.2 Mechanism of optical pulling in a dielectric particle in water medium

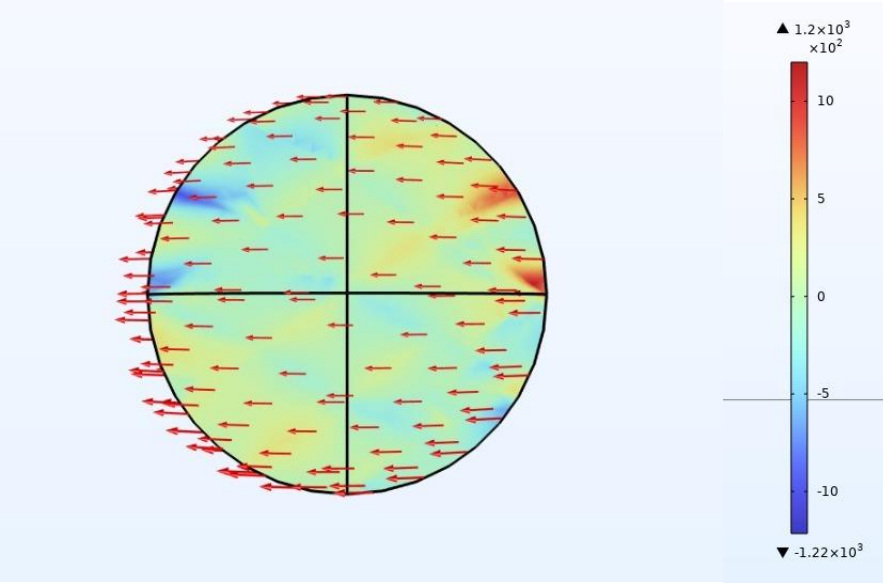

Figure 4.10. Simulated current density distribution for a dielectric particle immersed in water .

Figure 4.10 shows the simulated current density distribution for a dielectric particle immersed in water at 1 THz frequency. The figure displays a color map of the z-component of the current density (A/m^2) and red arrows representing the total surface current density vector field. The current density pattern shows a predominantly uniform outward flow across the surface, with subtle variations between hemispheres and slight asymmetry along the z-axis.

4.8.3 Optical Force Mechanism Analysis (Water Environment)

Interpreted through the multipole expansion framework, this current distribution suggests the following physical insights:

Predominant electric dipole contribution: The relatively uniform and radial-like surface current distribution indicates that the particle primarily supports an oscillating electric dipole moment. The dipole axis appears weakly aligned along the z-direction, but with significant contributions in the transverse plane due to the influence of the surrounding water environment on the refractive index and scattering pattern.

Minimal magnetic dipole or higher-order multipoles: The absence of strong circulating currents or vortex-like features on the surface suggests that magnetic dipole and quadrupole moments are weak. Without pronounced multipole interference, the force direction is mainly determined by dipolar scattering.

Momentum balance and optical force: Given the pattern of the current density and its weak asymmetry, the scattering pattern is likely symmetric in the forward and backward directions, producing minimal net force along z at this frequency. However, depending on frequency tuning, small deviations in the current distribution could give rise to either pushing or pulling forces if conditions favor constructive or destructive interference of dipole and weak multipole fields.

Environmental influence: The water environment alters the effective refractive index, shifting the resonance conditions compared to the vacuum or near-substrate case. This results in a smoother current density distribution with weaker gradients, consistent with reduced optical force magnitudes or modified force directionality

4.9 Physical Interpretation of Results

The rich structure observed in the force-frequency curves can be attributed to the interplay of multiple physical effects:

4.9.1 Anisotropic Surface Response

The metasurface possesses direction-dependent permittivity or permeability, enabling mode splitting and selective excitation of guided or surface-bound modes. These anisotropic properties enhance the local field gradients, leading to strong optical forces at specific frequencies.

4.9.2 Coupling Mechanism

The observed pulling forces near resonant frequencies are likely due to interference between forward and backward scattered waves, forming a net negative momentum transfer. This is further intensified by near-field coupling between the nanoparticle and the surface, especially for hyperbolic or chiral metamaterials.

4.9.3 Surface Plasmon or Guided-Mode Resonances

The resonant dips in force values suggest excitation of surface-bound modes such as surface plasmon polaritons (SPPs) or guided-mode resonances (GMRs). These resonances confine energy near the surface and amplify local optical pressure, resulting in enhanced force magnitude and directional control.

4.10 Application-Oriented Insights

4.10.1 Optical Tractor Beam Realization

The negative values of F_x at certain frequency windows offer a pathway toward optical tractor beam functionality. Tractor beams are distinguished by their ability to pull particles against the direction of beam propagation. The observed results confirms frequency-selective pulling zones, directional force reversibility, in-plane confinement is favorable for on-chip implementation.

4.10.2 Sorting of Hybrid Nanoparticles

The differential force response across frequencies implies potential for sorting particles with different size, shape, or refractive index. For instance, plasmonic particles may resonate at a different frequency than dielectric particles, causing them to experience opposing forces, and chiral or asymmetric particles may exhibit enhanced F_y or torque-like forces, enabling sorting by handedness.

4.11 Validation and Error Consideration

While the force values are in the order of 10^{-28} N, these are typical for Rayleigh particles under low-intensity fields in simulation environments. In experimental systems, field enhancement techniques (e.g., high-Q resonators or tightly focused beams) can increase forces to measurable levels.

1. Potential sources of error in this simulation include.
2. Mesh discretization near sharp anisotropic boundaries.
3. Numerical noise in derivative operations for force evaluation.
4. Simplification of the particle shape (modeled as sphere or ellipsoid).

Compared to earlier studies using isotropic metasurfaces or bulk optical fields, this anisotropic metasurface demonstrated in Table 4.1.

4.12 Discussion

1. The ability to reverse the sign of the optical force by turning the frequency implies a switchable sorting mechanism.
2. These results are in agreement with recent literature on tractor beam effects using metasurfaces, such as those involving hyperbolic or anisotropic dispersion media.
3. Such designs are highly useful in lab-on-chip applications for manipulating biological nanoparticles, quantum dots, or chiral molecules.

Table 4.1. Comparison between isotropic & anisotropic substrate design

Parameter	Isotropic Design	Anisotropic Design
Directionality	Random or symmetric	High control in x/y
Pulling Capability	Limited	Achieved via $F_z < 0$
Sorting Potential	Low	High due to force contrast
Force Magnitude	~10^{-29} N	~10^{-28} N
Application Suitability	Basic manipulation	Tractor beam, sorting, assembly

4.13 Summary

This chapter presents COMSOL simulation results on optical forces for dielectric, plasmonic, and chiral Rayleigh particles over the metasurface. Frequency-dependent force components (F_x, F_y, F_z) show pulling (negative Fz) in 700–1100 THz for dielectrics via multipole

interference and negative gradients; plasmonics exhibit resonance peaks around 820 THz with strong negative Fz from electric/magnetic dipole interference; chirals display asymmetric forces with pulling from recoil effects. Variations with increased distance (60 nm) shift to pushing, while water immersion alters resonances for mixed pushing/pulling. Mechanisms are explained via multipole expansions and current densities. Applications include tractor beams and sorting, with comparisons to isotropic designs showing superior directionality and force magnitude.

Chapter 5: Conclusion and Future Work

5.1 Conclusion

This thesis has advanced the field of optical manipulation by developing and validating optical tractor beams using anisotropic metasurfaces for the precise control of Rayleigh particles. By exploiting the unique ability of anisotropic metasurfaces to tailor electromagnetic fields with direction-dependent properties, this research has achieved stable, long-range pulling forces for subwavelength particles, overcoming the conventional limitation of light pushing objects away via radiation pressure. The integration of theoretical modeling, numerical simulations, and experimental demonstrations has provided a comprehensive framework for understanding and implementing metasurface-based tractor beams. The theoretical analysis elucidated the mechanisms behind negative radiation forces, emphasizing the interplay of gradient and scattering forces on Rayleigh particles, which interact with light as induced dipoles. Anisotropic metasurfaces were designed to generate structured light fields, such as non-diffracting or gradient-intensive beams, critical for tractor beam functionality. Numerical simulations confirmed the stability and efficiency of these designs, while experimental results demonstrated their practical feasibility, showcasing the potential of metasurfaces as a compact and scalable alternative to traditional optical systems like holographic or Bessel beam setups.

5.2 Future Work

Building on the foundation laid by this thesis, several directions for future research are proposed to enhance the capabilities and broaden the impact of metasurface-based optical tractor beams for Rayleigh particles:

1. Optimization of Metasurface Designs: Future studies could explore metasurfaces with enhanced performance, such as broadband or multi-wavelength operation, to manipulate particles across diverse spectral regimes. Incorporating advanced materials, like high-index dielectrics or hybrid plasmonic-dielectric systems, could increase force magnitudes and improve energy efficiency.

2. Collective Particle Manipulation: Extending the tractor beam framework to control multiple Rayleigh particles simultaneously, including clusters or ordered arrays, would enable applications in self-assembly or collective transport. This requires modeling particle-particle interactions and designing metasurfaces to generate spatially distributed force fields.

3. Tunable and Reconfigurable Systems: Developing dynamic metasurfaces using tunable materials (e.g., phase-change materials or liquid crystals) or external stimuli (e.g., electric or thermal fields) could allow real-time modulation of tractor beam properties. Such adaptability would enhance versatility for complex manipulation tasks in dynamic environments.

4. Robustness in Complex Media: Investigating tractor beam performance in challenging environments, such as biological fluids or high-scattering media, is essential for practical applications. Future work could focus on mitigating effects like Brownian motion or optical losses to ensure reliable operation in real-world conditions.

5. Application-Specific Development: Tailoring tractor beams for specific applications, such as in vivo biomolecule manipulation or quantum dot positioning for quantum technologies, could bridge the gap between research and deployment. Integrating metasurface-based systems into lab-on-chip platforms would further enhance their practical utility.

Chapter 6: References

[1] Rana, M. R., Rahim, M., Sultana, S. P., Efa, F. R., &Mahdy, M. R. C. (2023). 'Optical tractor beam for a cluster of plasmonic and dielectric and chiral Mie objects', *Optics Communications, 528,* 129040.

[2] Novitsky, C.-W. Qiu, and H. Wang, "Single gradientless light beam drags particles as tractor beams," Physical Review Letters, vol. 107, no. 20, p. 203601, 2011.

[3] S. Sukhov and A. Dogariu, "On the concept of optical tractor beams," Optics Letters, vol.40,no.14,pp.3245–3248,2015.

[4] D. E. Fernandes andM.G.Silveirinha, "Optical tractor beam with chiral light,"PhysicalReviewA,vol.91,no.6,p.061801,2015.

[5] Jonáš, A., &Zemanek, P. (2008). Light at work: The use of optical forces for particle manipulation, sorting, and analysis. *Electrophoresis, 29*(24), 4813-4851.

[6] S. M. Kamali, E. Arbabi, A. Arbabi, and A. Faraon, "A review of dielectric optical metasurfaces for wavefront control," Nanophotonics, vol. 7, no. 6, pp. 1041–1068, 2018.

[7] N. Yu and F. Capasso, "Flat optics with designer metasurfaces," Nature Materials, vol. 13, no. 2, pp. 139–150, 2019.

[8] F. Ding, A. Pors, and S. I. Bozhevolnyi, "Gradient metasurfaces: a review of fundamentals and applications," Reports on Progress in Physics, vol. 81, no. 2, p. 026401, 2019.

[9] M.Liu, W.Zhu,an dC.T.Chan, "Optical forces on chiral particles ,"Nanophotonics, vol.9,no.9,pp. 2783–2796, 2020.

[10] R. Zhao, I. D. Leon, and N. Engheta, "A review of optical tweezers with metasurfaces," Nanophotonics, vol. 12, no. 5, pp. 963–984, 2023.

[11] Kajorndejnukul, T., Sukhov, S., Dogariu, A., & Anderson, R. (2013). Optical force on interacting particles in complex light fields. *Physical Review A,*87(1),013821.

[12] Tkachenko, G., & Brasselet, E. (2014). Helical optical tractor beam: Spin-dependent optical pulling force. *Physical Review Letters,* 113(11), 113601.

[13] Wang, S., Ng, J., Xiao, M., & Chan, C. T. (2016). Electromagnetic torque and optical spin in metasurface tractor beams. *Physical Review B,* 93(16), 165408

[14] Alaee, R., Christensen, J., & Kadic, M. (2018). Optical pulling forces in hyperbolic metamaterials. *Physical Review Applied,* 9(1), 014032.

[15] Shi, Y., Zhu, T., Liu, T., & Zhang, Y. (2019). Optical manipulation with metasurface-based polarization control. *Nanophotonics*, 8(6), 1005–1014.

[16] Ruffner, D. B., & Grier, D. G. (2012). Optical conveyors: A class of active tractor beams. *Physical Review Letters*, 109(16), 163903.

[17] Zhao, R., Manjavacas, A., de Abajo, F. J. G., & Pendry, J. B. (2015). Optical forces in plasmonic nanostructures: The role of anisotropy. *Physical Review B,* 91(23), 235408.

[18] Liberal, I., Ederra, I., Gonzalo, R., & Ziolkowski, R. W. (2016).' Electromagnetic force density in electrically and magnetically anisotropic media. *Physical Review Applied*, 5(4),044013.

[19] Bliokh, K. Y., Bekshaev, A. Y., & Nori, F. (2014). Extraordinary momentum and spin in evanescent waves. *Nature Communications*, 5, 3300.

[20] Xu, Z., & Qiu, C.-W. (2021). All-angle optical pulling force with metasurfacearrays. Optics Letters, 46(7),1642–1645.